IOPscience iopscience.iop.org

Home Search Collections Journals About Contact us My IOPscience

An electron-beam plasma source and geometry for plasma processing

This article has been downloaded from IOPscience. Please scroll down to see the full text article.

1993 Plasma Sources Sci. Technol. 2 100

(http://iopscience.iop.org/0963-0252/2/2/005)

View the table of contents for this issue, or go to the journal homepage for more

Download details:
IP Address: 192.17.144.173
The article was downloaded on 23/12/2012 at 20:58

Please note that terms and conditions apply.

Plasma Sources Sci. Technol. 2 (1993) 100–105. Printed in the UK

An electron-beam plasma source and geometry for plasma processing

Ken D Schatz and David N Ruzic
University of Illinois, 103 S. Goodwin Avenue, Urbana, IL 61801, USA

Received 13 August 1992, in final form 30 November 1992

Abstract. The operation of an electron-beam plasma source and its application as a secondary source of ionization in a radio frequency- (RF) powered reactive-ion-etching (RIE) reactor is investigated. RF-powered RIE is an important tool in the manufacture of semiconductor devices. One aspect of RF RIE is its ability to produce a DC substrate potential on insulating as well as conducting substrates. Substrate potential is an important determinant of etch anisotropy. However, traditional RF RIE reactors can only be operated over a limited range of parameter space. Ion flux, neutral radical flux and ion energy must all be controlled with only two independent variables: RF power and pressure. Expanded and precise control over process parameters is becoming more important as device structures are made smaller and less damage tolerant. Process control may be enhanced by the addition of an alternative source of power.

The experimental arrangement is designed to investigate these possibilities. As a test case, the system is utilized to etch patterned silicon wafers with SF_6 gas. Etch rate, etch uniformity and DC bias potential versus RF power and beam current are presented. Electron-gun generated contamination is addressed and several solutions are reported.

1. Introduction

The operation of an electron-beam plasma source and its application as a secondary source of ionization in a radio frequency- (RF) powered reactive ion etching (RIE) reactor is investigated. RF-powered RIE has been a useful dry etching technique for several decades. An important attribute of RF RIE is the formation of a DC self-bias potential on the powered electrode. This produces the unidirectional ion flux required for anisotropic etching. Secondary attributes include the simplicity of single power supply operation, relative ease in the scaling of systems from single to multi-wafer designs, and no requirement for large electromagnets. However, since the DC self-bias potential and the plasma are both created by the same power supply, the ion energy and ion flux or neutral radical flux at the substrate are not independently controllable. This lack of control becomes more of a problem as circuit element packing densities are increased and device structures made less damage tolerant. ULSI circuit manufacture would benefit from RIE systems with more process flexibility and, specifically, higher radical fluxes with lower ion energies than are presently available with a single power supply RF-driven design.

Process control is increased by decoupling the plasma source from the source of DC self-bias. Past studies of decoupled systems have investigated RF triodes [1], or combinations of an RF-powered wafer chuck with an ECR [2], or RF helicon [3] plasma source. The experimental investigation presented here details the operation of an electron-beam plasma source and explores its coupling into an RIE system composed of a combined electron-beam plasma and RF-powered wafer chuck. The RF power produces a DC self-bias on the substrate, increases the plasma density and affects the electron energy distribution. As a test case, the system was employed to etch silicon in SF_6 at 50 mTorr. Results presented cover effects on the substrate potential caused by variations in beam current and RF power, etching uniformity versus distance from the electron gun and methods for eliminating contaminants sputtered from the gun cathode.

Combined electron-beam- and electromagnetic-field-driven plasmas are referred to as electron-beam sustained discharges (EBSD). EBSD have been investigated for use in high efficiency CO_2 [4] and excimer [5] lasers. The efficiency advantage stems from a decrease in the bulk electron temperature for a given plasma density in an EBSD driven plasma as compared with a DC electric-field- or electromagnetic-field-only driven plasma. Lowering the electron temperature results in enhanced rates of excitation and molecular dissociation relative to the rate of ionization. While increasing the rate of excitation is beneficial in a laser, increased neutral radical production, i.e. dissociation, is beneficial to etching as well as other plasma processing techniques. EBSD may have other advantages for plasma processing systems as well. These

0963-0252/93/02100+06 $07.50 © 1993 IOP Publishing

include relative ease in controlling process uniformity through choice of electron gun location and geometry, and relatively simple and low cost power supplies and power connections.

2. Experiment

The cold-cathode electron gun utilized for the majority of the data presented is shown schematically in figure 1. The cathode face is aluminum, and the active emitting area of the cathode is defined by a 6.4 × 1.3 cm slot cut through a quartz insulating plate. The 3 mm thick quartz plate is mounted 1 mm in front of the cathode face and is held in place by silica cement. Silica cement also insulates the sides and back of the cathode. The small 1 mm gap between quartz and cathode was found to prevent arcs which formed around the edges of the active cathode area when no gap, or too large a gap, was present.

The operation and characteristics of cold cathode electron guns are well described in reference [6]. Briefly, a beam-driven plasma can be broken down into three regions as shown in figure 2: region 1, the cathode fall region, characterized by an intense electric field; region 2, the energy thermalization region for moderate energy electrons, characterized by an electric field free region of high plasma and radical densities; region 3, the high energy electron thermalization region, a field-free region where beam flux and plasma density gradually decrease with distance from the gun. The moderate energy electrons in region 2 were born in ionizing collisions in the cathode fall region at some distance from the cathode surface, hence they cannot acquire the full beam energy. The high energy electrons of region 3 were born at the cathode surface by the process of secondary electron emission. These electrons are accelerated to nearly the full cathode potential, typically suffering only 0–5 strong inelastic collisions over the length of the cathode fall.

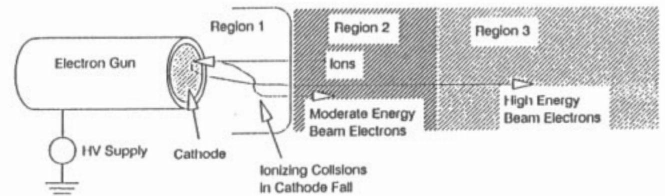

Figure 2. Schematic representation of a cold cathode electron-beam generated plasma.

Note that the separation between regions 2 and 3 is blurred by the diffusion of plasma and radicals from 2 into 3. The effects of this diffusion are evident in the etch uniformity data presented in the next section.

The cold cathode electron gun is located on the axis of the chamber with the cathode face 8.25 cm from the near chamber end plate and 2.1 cm from the near edge of the wafer chuck. The short distance between gun and chuck does not provide good etch uniformity but instead allows measurement of the etch rate at various positions along the beam and hence provides the data necessary to design future equipment. The beam passes just above the substrate and continues on to the far chamber end plate where excess energy is absorbed in a water cooled, stainless steel beam stop. The electron gun is also water cooled.

A schematic diagram of the experimental etching set-up is shown in figure 3. The chamber is an aluminum cylinder 28 cm long with a 30.5 cm inner diameter (ID). Two 15 cm ID ports are located on opposite sides of the cylinder, midway between its end plates. A viewport seals one of the ports. The other port is closed with a flange which includes a feed-through for the RF-powered wafer chuck.

Sulphur hexafluoride (SF_6) gas is metered into the chamber at 15 ± 0.2 SCCM through a mass flow controller. A chamber pressure of 50.0 ± 3.0 mTorr is maintained by adjusting a poppet valve located between the chamber and mechanical pump.

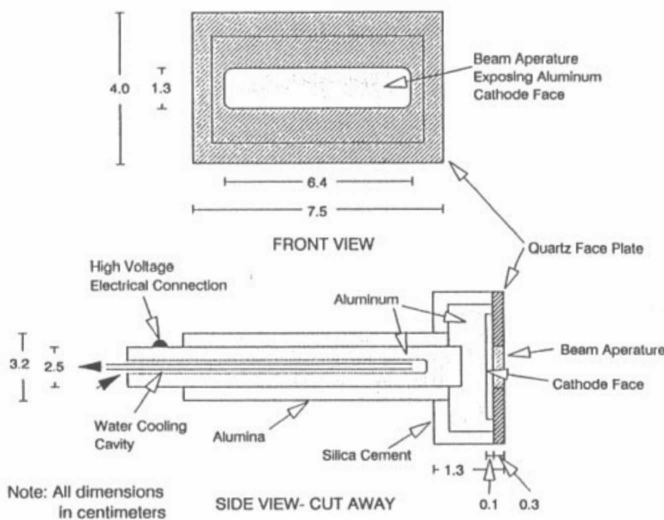

Figure 1. Schematic diagram of the aluminum cathode electron gun. The beam originates on the portion of the cathode face exposed to the plasma by the beam aperture.

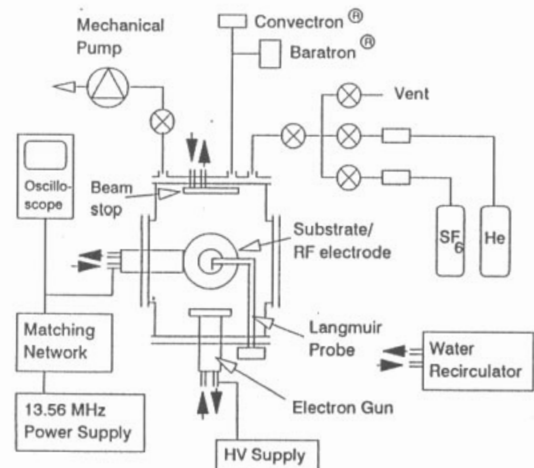

Figure 3. Schematic diagram of the experimental set-up. Note that cooling water connections are represented by solid arrows.

The wafer chuck is positioned in the centre of the chamber. The chuck is a 11.5 cm diameter, 1.3 cm thick stainless steel disc with internal water cooling passages. Patterned silicon substrates (50 mm diameter, ⟨100⟩ p-type with 6 Ω-cm) are clamped to the chuck with five 1 mm thick stainless steel clips. These clips are screwed down flush against the chuck and wafer and are positioned around the wafer so as not to block any part of the electron beam. The wafer chuck can be rotated so that the beam impinges directly onto the wafer. For the experiments described here, however, the chuck is positioned such that the beam skims just over the top of the wafer with the beam axis perpendicular to the wafer surface normal.

The wafer chuck is driven with a 13.56 MHz power supply through a matching network. The output capacitor of the matching network allows the substrate to acquire a DC self-bias during RF operation or a floating potential during electron beam only operation. The RF voltage and self-bias were measured across a 100-to-1 voltage divider with a Tektronics, model 7704A oscilloscope.

The electron-beam plasma was diagnosed with a Langmuir probe. The probe is attached to a manipulator arm connected to a rotary feedthrough. The manipulator allows the probe to be swept across the plasma from the chamber wall to just above the centre of the wafer in a plane perpendicular to the beam axis.

The Langmuir probe is constructed of a length of 0.25 mm diameter tungsten wire extending 6.5 mm beyond a 1.6 mm OD alumina tube. The tungsten wire extends out at 90° to the alumina tube and is designed so that the axis of the exposed wire is oriented along the direction of the electron beam, thus limiting the direct collection of beam electrons by the probe. Also, with gas pressure of only 50 mTorr the number of beam-neutral collisions within the probe sheath is small. The probe measures the bulk plasma properties, not the energetic beam component.

3. Results

The electron beam starts at the cathode with a 5.7 × 0.6 cm cross section, not 6.4 × 1.3 cm as defined by the slotted quartz plate, due to a plasma sheath which forms on the quartz. The beam diverges slowly with distance from the cathode: at 10 cm from the cathode the cross section is approximately 7 × 2 cm.

Cathode total current (electron and ion currents) versus cathode voltage data are shown in figure 4. Data are presented for operation in pure SF_6 and pure O_2. By comparison, at 2.0 kV in 50.0 mTorr of He, the cathode current density is only $0.02 \pm 0.005\,\mathrm{mA\,cm^{-2}}$. Previous studies on the effects of different gases on cold-cathode current densities have demonstrated that the presence of a thin layer of insulating material on the cathode will greatly enhance its secondary emission coefficient, and hence the achievable cathode current density [7, 8]. This enhancement effect is clearly seen with either O_2 or SF_6 as the working gas due to the formation of a thin oxide or fluoride layer on the cathode. While an enhanced cathode current density can produce a higher plasma density, the insulating material formed is non-volatile and, when sputtered from the cathode, is a possible source of contamination. Contaminants of this form were observed on the substrate. Their potential elimination is addressed below.

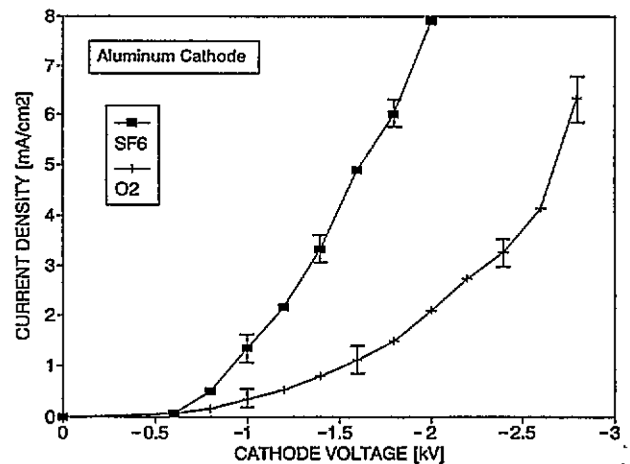

Figure 4. Electron-gun cathode current density versus gun voltage for an aluminum cathode in 50 mTorr of SF_6 or O_2.

Langmuir probe data were taken for an SF_6 beam plasma, no RF power, at a distance of 10 cm from the cathode. Correct interpretation of the probe data to provide absolute numbers is hindered by the effects of the electronegativity of the SF_6 gas and, to a lesser extent, by the beam. However, changes in the $I-V$ characteristic with beam current and position do provide relative measurements. Data show plasma densities within the beam of the order of $10^{10}\,\mathrm{cm^{-3}}$ for a beam current of 65.0 ± 2 mA and of the order of $10^{9}\,\mathrm{cm^{-3}}$ for a 25.0 ± 2 mA beam. These plasma densities are roughly a factor of 100 greater than the density of the high energy beam electrons due to the secondary ionizations produced by the beam. Crossing the beam edge boundary from inside the beam to outside, the plasma density and floating potential fall off gradually. However, the plasma potential changes rapidly at the beam edge boundary. With a 25.0 ± 2 mA, 1.95 ± 0.07 kV beam, the plasma potential changes over a distance of approximately 3 cm from -5.0 ± 0.5 V to 0.0 ± 0.2 V, the floating potential decreases from -9.0 ± 0.5 V to -6.0 ± 0.2 V, and plasma density falls by approximately one half.

Data showing the effects of beam current and RF power on substrate potential are presented in figure 5. The data show that over the range of RF power investigated, the substrate potential due to the combined beam and RF can be decoupled into beam only and RF only parts. The substrate potential drops (becomes more negative) with RF power linearly with a slope of -0.4 ± 0.03 DC volts per RF Watt. The variation of the substrate potential with beam current is independent of RF power and drops exponentially with beam current roughly as: $V_{sub}\,(\mathrm{V}) = -\exp(I_{beam}\,(\mathrm{mA})/16.2)$. The result-

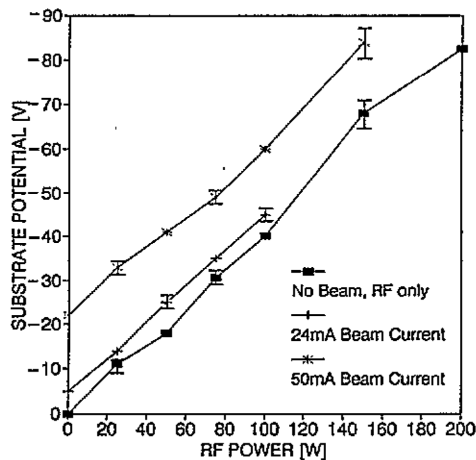

Figure 5. Substrate DC bias potential versus RF power for constant beam currents of 0, 24 mA, and 50 mA.

ant substrate potential for a combined beam and RF plasma is then the sum of these two terms. The measured plasma potential is close to zero for all the cases presented, this due to the large grounded surface area and the electronegativity of SF_6 gas. Since the sheath thickness is less than, but of the same order of magnitude as, the ion mean free path, the substrate potential indicates the maximum ion energy incident on the substrate.

Silicon etch characteristics were investigated on wafers patterned with a repeated series of 5, 3 and 2 μm spaced lines formed in 1450J resist. Etch rate and substrate potential data taken for a 24 mA, 2 kV beam, 50 W RF, and a combination of the two are presented in table 1. As noted above, the maximum ion energy is only a few electron-volts different from the DC self-bias potential. For the conditions investigated in table 1, the combined beam and RF etch rate is approximately equal to the sum of the beam only and RF only rates. This is due to the rapid etching of silicon by neutral atomic fluorine. The atomic fluorine density scales linearly with plasma density as long as the ionization fraction is significantly less than one. The DC self-bias also sums, however the etch rate increase is not a result of the added potential but due to an increased plasma density. Effects on etch rate caused by differences in ion energy can be pronounced with ion activated etchants [9] such as chlorine-containing gases or low-temperature SF_6.

SEMs of the etched pattern show contamination deposited on the bottoms of the etched troughs. This material is a non-volatile aluminum and fluorine compound [10] resulting from material sputtered from the electron gun cathode. The material is only weakly bound to the silicon. It is formed in the gas phase or on the cathode and then rains down on the silicon as small particles. These particles act as etching masks resulting in a roughened etched surface with small etch pits.

Table 1. Silicon substrate etch rate and DC self-bias data for several combinations of electron-beam powers and RF power.

Electron beam				
Voltage (kV)	Current (W)	RF power (W)	Etch rate (nm min^{-1})	DC self-bias (V)
2.1	24.0	0	115.0	−8.0
0	0	50.0	116.0	−17.0
2.1	24.0	50.0	236.0	−25.0

Figure 6 presents etch rate data as a function of distance from the electron gun cathode for 24 mA and 50 mA beam only plasmas. Note that within 5 cm of the gun, the apparent etch rate increases with distance. This is due to a high rate of deposition of the contaminant aluminum compound. It is the decrease in contaminant deposition with distance which causes the increase in etching rate. At distances beyond 5 cm, the etch rate decreases rapidly at first, approximately as 1/distance, and then more slowly. A 1/distance rate decrease is expected if all of the ions and radicals were born in the high plasma density region just outside of the cathode fall (region 2 in figure 2) and diffused outwards with a recombination length scale greater than the cathode-to-wafer distance. For distances greater than 16 cm, the etch rate is little affected by species diffusing from this region, and a gradual decrease in etch rate parallels the slow decrease in plasma density in region 3 of the beam plasma.

In order to reduce the transport of contaminants from the electron gun to the substrate and to reduce the diffusion of plasma species born in region 2, a shield was installed between the gun and the wafer chuck. The shield arrangement as tested is shown in figure 7. The shield is a 1.6 mm thick sheet of stainless steel with a 1 × 6.4 cm window cut out. The shield is positioned 2 cm in front of the gun with the window aligned with the active area of the cathode. The short 2 cm cathode-to-shield separation distance is not optimal, but for this exploratory study the cathode-to-wafer chuck distance was kept the same as in the previous experiments. The resulting etch rate versus distance data are presented in figure 8. Note the overall lower magnitude but more gradual decrease with dis-

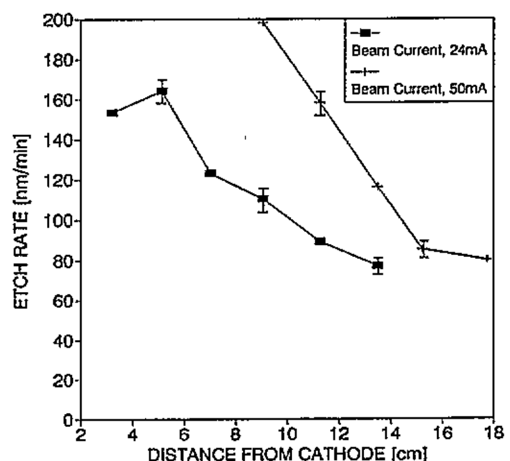

Figure 6. Silicon etch rate versus distance from cathode for 24 mA and 50 mA beam currents and no RF power in 50 mTorr SF_6.

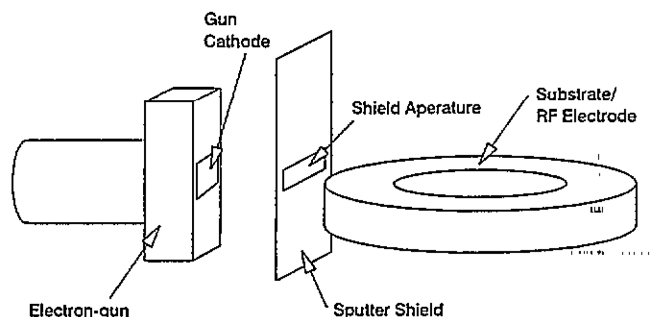

Figure 7. Schematic diagram of the experimental arrangement with sputter shield between gun and substrate.

tance in rate as compared with figure 6. These results show the effectiveness of the shield in excluding much of the region 2 products from the wafer area. Photomicrographs of the patterned wafers etched in a 2.1 kV, 24 mA beam, no RF, show a marked decrease in contamination as compared with the non-shielded results. Under high magnification the surfaces of the etched troughs appear as approximately equal areas of clean silicon and small islands of contamination, 25 nm × 250 nm in area and 25 nm tall.

An alternative method of eliminating gun-generated contaminants would be to use a cathode fabricated from a material which, when sputtered, forms volatile compounds. Suitable materials might be graphite or silicon. An electron gun with a silicon cathode face was tested, and SEM microphotographs of etched wafers show no indication of surface contamination. Beam current versus beam voltage data for the silicon cathode gun are presented in figure 9. Note that at 2 kV the gun current is 25% less than that of the aluminum cathode gun. Although the silicon cathode current is lower, it is sufficient for use as a practical cathode material. Also, the discharge is observed to be stable to higher gun voltages for the silicon cathode. The etch rate of the silicon cathode face was measured to be 1.0 ± 0.5 μm min^{-1} after

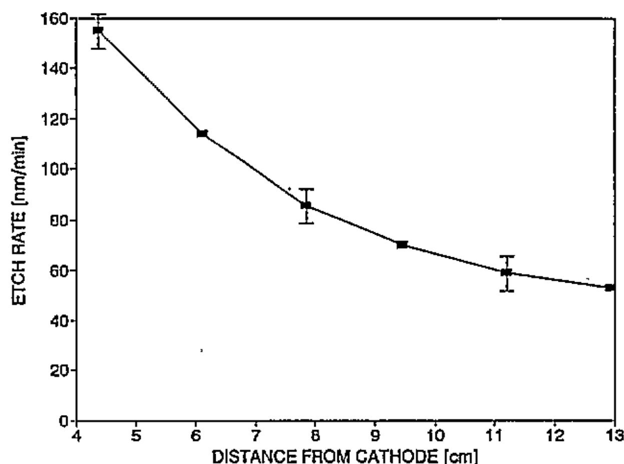

Figure 8. Silicon etch rate with sputter shield in place for a 24 mA beam in 50 mTorr SF_6.

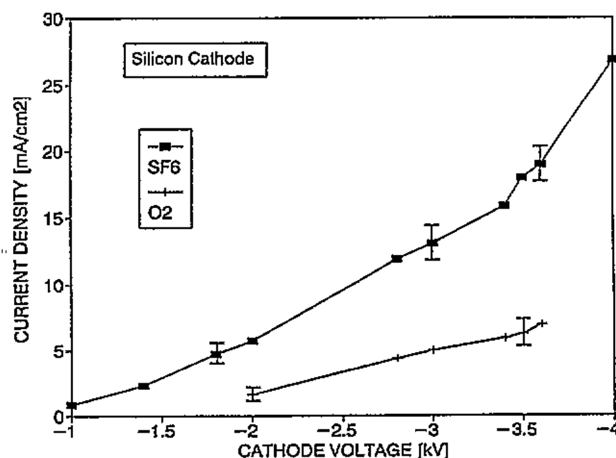

Figure 9. Electron-gun cathode current density versus gun voltage for a silicon cathode in 50 mTorr of SF_6 or O_2.

operation at 1–4 kV; the cathode etch rate for the aluminum cathode gun is orders of magnitude lower.

4. Discussion

In analysing the beam-powered plasma results it was noted that the beam edge diverges outwards at a 4° angle from the cathode normal even though the cathode face is planar. Hence a small fraction of the beam electrons do impinge on the silicon surface. Beam spreading can be reduced either by installing a beam-shaping aperture located a distance from the cathode (this effect is observed when the sputter shield is in place) or by cupping the cathode face so as to electrostatically focus the beam [7].

Accurately defining the beam geometry and, most importantly, its distance above the substrate surface could be beneficial in practical beam driven systems. Controlling the height of the bottom edge of the beam above the substrate would allow for adjustment of the ion flux to neutral radical flux ratio and the ion energy. This is evident from the rapid variation with distance from the beam edge of the Langmuir probe data.

Substrate potential is determined by the sum of the potentials due to the beam only and the RF only. Hence control is provided by varying the RF power, beam current, or beam height. This allows for a great deal of flexibility in selecting operating parameters.

The SF_6 Si RIE etching experiment was chosen only as a test application for this plasma source. The etch rate data of figures 6 and 8 indicate the need for larger or multiple cathodes in order to increase plasma density and etch rate. Plasma density can also be increased by use of pairs of opposing gun cathodes to provide electrostatic confinement of the beam electrons or a magnetic field arrangement to confine the bulk plasma.

Etch uniformity can be estimated by fitting the data of figure 8 with an equation derived by assuming a diffusion source located at the sputter shield aperture and a constant beam-driven plasma generation term. This

model predicts that in order to achieve a 3% etch uniformity over a 6 in wafer a pair of opposing guns, each with a sputter shield, be positioned with at least 30 cm between each cathode and the wafer centre. Similar uniformity problems in electron-beam driven excimer lasers have been handled by employing opposing guns. The arrangement is referred to as double-sided injection or pumping [11]. Adding more pairs of guns and focusing each beam to contract, and so intensify, over the wafer will reduce the needed cathode to wafer separation still further. Gun generated contamination can be minimized by fabricating the cathodes from silicon or possibly graphite.

In a practical system, etch anisotropy and selectivity can be controlled by proper selection of process gases. In SF_6, anisotropic etching with good selectivity is achieved by cooling the substrate [12] to temperatures near $-30\,°C$.

5. Conclusions

An electron-beam plasma source of use in plasma processing has been designed and tested as a combined electron beam and RF powered RIE system. The experimental arrangement was chosen to investigate gun characteristics and the synergistic effects between the plasma sources: the effects of beam current and RF power on substrate potential, etch rate as a function of distance from the electron gun, and possible sources of wafer contamination. Experimental results indicate that substrate potential contributions due to RF power and beam current are independent and sum linearly in combined beam/RF discharges. Also the requisite etch uniformity can be realized by sufficiently increasing the gun-to-substrate distance to shield the substrate from the intense plasma generated near the electron gun. Gun derived contamination can be alleviated by utilizing a silicon cathode.

Acknowledgments

The authors are grateful for the generous support in equipment and funding from the IBM Corporation, INTEL and the INTEL Foundation. We also wish to thank Mr Dean Swofford for providing technical support and Ms Rebecca Priest for providing editorial assistance.

References

[1] Bogle-Rohwer E, Gates D, Hayler L, Kurasaki H and Richardson B 1985 Wall profile control in a triode etcher *Solid State Technol.* **28** 251

[2] Suzuki K, Ninomiya K, Nishimatsu S and Okudaria S 1985 Radio-frequency biased microwave plasma etching technique: a method to increase SiO_2 etch rate *J. Vac. Sci. Technol.* **B 3** 1025

[3] Perry A and Boswell R 1989 Fast anisotropic etching of silicon in an inductively coupled plasma reactor *Appl. Phys. Lett.* **55** 148

[4] Basov N and Danilychev V 1986 Condensed- and compressed-gas lasers *Sov. Phys.–Usp.* **29** 31

[5] Kushner M and Pindroh A 1986 Discharge constriction, photodetachment, and ionization instabilities in electron-beam-sustained discharge excimer lasers *J. Appl. Phys.* **60** 904

[6] Shi B, Meyer J, Yu Z and Collins G 1986 Energy spectrum of an abnormal glow discharge created electron beam *IEEE Trans. Plasma Sci.* **14** 523

[7] Hurley R and Holliday J 1978 Electrode surface effects in the high voltage glow discharge *Vacuum* **28** 453

[8] Rocca J J, Meyer J D, Farrell M R and Collins G J 1984 Glow-discharge-created electron beams: cathode materials, electron gun design, and technological applications *J. Appl. Phys.* **56** 790

[9] Coburn J W 1982 Plasma-assisted etching *Plasma Chem. Plasma Process.* **2** 1

[10] Oehrlein L, Schad R and Jaso M 1986 Mechanism of silicon surface roughening by reactive ion etching *Surf. Interf. Analysis* **8** 243

[11] Rosocha L A and Riepe K B 1987 Electron-beam sources for pumping large aperture KrF lasers *Fusion Technol.* **11** 576

[12] Tachi S, Tsujimoto K and Okudaira S 1988 Low-temperature reactive ion etching and microwave plasma etching of silicon *Appl. Phys. Lett.* **52** 616